Applied Physics Letters ARTICLE scitation.org/journal/apl

Optical absorbance in multilayer two-dimensional materials: Graphene and antimonene

Cite as: Appl. Phys. Lett. **116**, 263102 (2020); doi: 10.1063/5.0010794
Submitted: 16 April 2020 · Accepted: 14 June 2020 ·
Published Online: 30 June 2020

Ashok Kumar,[1,2,a)] Geeta Sachdeva,[1] Ravindra Pandey,[1,a)] and Shashi P. Karna[3]

AFFILIATIONS

[1]Department of Physics, Michigan Technological University, Houghton, Michigan 49931, USA
[2] Department of Physics, School of Basic and Applied Sciences, Central University of Punjab, Bathinda 151001, India
[3]CCDC Army Research Laboratory, Weapons, and Materials Research Directorate, ATTN: FCDD-RLW, Aberdeen Proving Ground, Aberdeen, Maryland 21005-5069, USA

[a)]**Authors to whom correspondence should be addressed:** fashokku@mtu.edu and pandey@mtu.edu

ABSTRACT

Antimonene, one of the group V elemental monolayers, has attracted intense interest due to its intriguing electronic properties. Here, we present the optical absorption properties of atomically flat antimonene for which the directional bonds between Sb atoms appear to be analogous to C–C bonds in graphene. The results, based on first-principles density functional theory calculations, predict the absorbance in multilayer antimonene to be comparable or higher than that calculated for multilayer graphene. Specifically, the IR absorption in antimonene is significantly higher with a prominent band at about 4 μm associated with the dipole-allowed interband transitions. Furthermore, a strong dependence of absorbance on topology is predicted for both antimonene and graphene which results from the subtle variations in their stacking-dependent band structures. Our results suggest multilayer antimonene to be a good candidate material for optical power limiting applications in the IR region.

The optical properties of two-dimensional (2D) atomically thin layers have attracted a great deal of attention in recent years.[1] From the early measurements of nonlinear transmission and scattering[2] and two-photon absorption (TPA) on graphene[3] and four-wave mixing measurements on graphene flakes[4] to the measurements of the intensity-dependent refractive index of antimonene[5] and more recently 2D GeP,[6] there has been a surge in the experimental observations and theoretical calculations on the linear and nonlinear optical (NLO) properties of 2D layered materials. Several excellent reviews on the subject have recently appeared in the literature.[1,4,6–9] Among the 2D materials, such as graphene, boron nitride (BN), phosphorene, and antimonene, the latter offers several appealing properties for applications in optoelectronics and photonics devices. The theoretical calculations[10,11] have predicted 2D antimonene to be a narrow bandgap semiconductor with two configurations of monolayer antimonene, α-Sb, which has a puckered structure with two atomic sublayers with an indirect bandgap of ∼0.28 eV and β-Sb with a buckled hexagonal lattice and a slightly higher indirect bandgap of ∼0.76 eV. Note that β-Sb can be synthesized by various physical or chemical methods such as molecular-beam epitaxy, epitaxy growth, etc.[1,12–14] Moreover, unlike phosphorene, atomically flat antimonene can be grown on a lattice-matched Ag (111) substrate with hexagonal symmetry.[11,15] It, therefore, appears that sp^2 hybridized Sb atoms form a planar graphene-like antimonene in which the lone-pair electrons on adjacent sites likely form out-of-plane nonbonding orbitals (Fig. S1).

Since directional bonding between Sb atoms in the planar antimonene appears to be analogous to C–C bonds in graphene, it is of interest to examine the optical properties of multilayer antimonene vis-à-vis multilayer graphene. Here, we present the optical absorption spectra ranging from near-infrared (0.8–5.0 μm) to visible (400–740 nm). Both layer- and topology-dependence on the absorption spectra are investigated via a detailed analysis of the band structure.

Calculations were performed by the density functional theory (DFT) approach using the projector augmented wave (PAW) potentials as implemented in the Vienna *ab initio* simulation package (VASP). The exchange and correlation functionals were treated within the framework of generalized gradient approximation (GGA) given by the Perdew–Burke–Ernzerhof (PBE) functional.[16] Contributions from the van der Waals interactions were incorporated by using the Grimme's semi-empirical dispersive D2 term.[17] Additional details are given in the supplementary material, e.g., Figs. S2–S4.

Low-energy optical absorption can be measured via absorption spectroscopy[18–24] and calculated using the imaginary part of the dielectric function.[25–28] Here, the frequency-dependent dielectric matrix ($\epsilon_2(\omega)$) was calculated by the "sum-over-states" (SOS) method.[8] The fraction of photon energy ($E = \hbar\omega$) absorbed by a multilayer is given as

$$A(\omega) = \frac{\omega}{c}\epsilon_2(\omega)L_z, \quad (1)$$

where L_z is the length of a supercell in the z-direction and c is the speed of light. In this way, the calculated absorbance is independent of the size of a vacuum in the z-direction of the periodic supercell (Fig. S3, supplementary material), and is equivalent to the absorbance calculated using the expression $[\frac{4\pi\omega}{c}\alpha_2(\omega)]$[29] with α_2 being the imaginary part of the polarizability per unit area. For a multilayer system, thickness is equivalent to L_z, and is defined as a sum of the vacuum distance and interlayer distance. The dependence of $\epsilon_2(\omega)$ on the vacuum distance considered in calculations is displayed in Fig. S4, supplementary material. Note that dielectric functions are inversely proportional to the volume of the cell in a periodic super cell method [Eq. (1), supplementary material].

DFT calculations were first performed on multilayer graphene for which the experimental low-energy absorption spectrum is known in the literature.[11,30] In our work, we find the energetically preferred configurations to be AB-stacked for bilayer (2L), ABA-stacked for trilayer (3L), and ABAB-stacked for a quad-layer (4L) at the DFT (PBE) + D2 level of theory (Table S1, supplementary material). It is worth noting that multilayer graphene exhibits distinct optical conductivity for Bernal (ABA) and rhombohedral (ABC) stacking in infrared absorption spectroscopy measurements.[23] Further, trilayer-graphene also exhibits distinct electronic structures for different stackings (AAA, ABA, and ABC) as measured with NanoARPES[31] and calculated using the tight-binding method.[32]

The calculated optical absorbance properties of multilayer graphene in terms of absorbance are shown in Fig. 1. Here, 1L is a monolayer, 2L is an AB-stacked bilayer, 3L is an ABA-stacked trilayer, and 4L is ABAB-stacked quadlayer graphene. In the IR region, the absorbance of monolayer graphene is nearly constant (~2.3%), which agrees well with experiments[11,30] and the calculated results obtained using the imaginary part of polarizability per unit area.[29]

For graphene, the out-of-plane polarization component of the electromagnetic field for absorbance is nearly zero in the visible spectrum, suggesting that it is optically transparent (Fig. S5, supplementary material). On the other hand, the in-plane polarization component of the electromagnetic field for absorbance is large and is mainly attributable to the atomic thickness of monolayer graphene. The most prominent absorption band appears at ~4 eV (≈310 nm) (Fig. S5, supplementary material), which is consistent with the results of previous studies.[20] The increase in the intensity of the ~4 eV band with the number of layers is likely due to the availability of a larger number of bands associated with the interband transition at the M point (Fig. S6, supplementary material).

In the 1.77–3.1 eV (i.e., 700–400 nm) region, a relatively small increase in transmittance is predicted [Fig. S7(b), supplementary material] and is consistent with experiments.[18,31,33] As thickness increases, the nonlinear behavior of transmittance can be seen in multilayer graphene. For $\lambda = 300$ nm and 800 nm [Figs. S7(c) and S7(d),

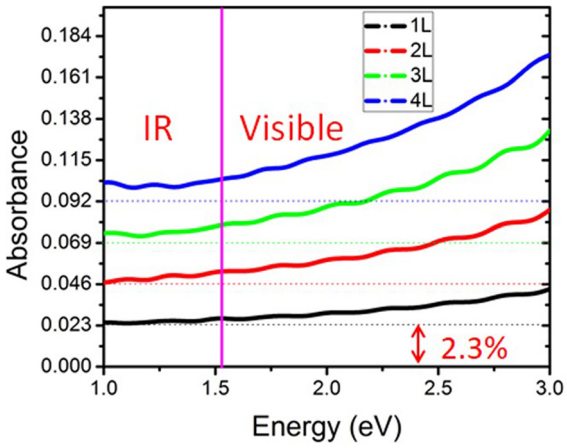

FIG. 1. Multilayer graphene: in-plane polarization component of the electromagnetic field for absorbance as a function of the number of layers (1L-monolayer, 2L-AB-stacked bilayer, 3L-ABA-stacked trilayer, and 4L-ABAB-stacked quadlayer).

supplementary material], a linear decrease in transmittance in going from monolayer to bilayer is noticed. Beyond n = 2, the transmittance shows a small nonlinearity which is relatively pronounced for 300 nm. The calculated results affirm the observation of the nonlinear behavior of transmittance of white light for five-layer graphene.[18] Overall, the transmission was reduced to ≈79% for 800 nm, ≈74% for 532, and ≈40% for 300 nm in ABAB-stacked 4L relative to that of the monolayer.

Next, we calculate the frequency-dependent refractive index given by the expression, $n(\omega) = \frac{1}{\sqrt{2}}\left[\epsilon_1 + \sqrt{\epsilon_1^2 + \epsilon_2^2}\right]^{1/2}$. The real part of dielectric function (ε_1) is obtained from the imaginary part of dielectric function (ε_2) using the Kramers–Kronig relations.[34] $n(\omega)$ exhibits a large increase in going from single to bilayer, then shows reduced increases upon successive addition of layers (Fig. S8, supplementary material).

The planar antimonene is semi-metallic[35] and, unlike graphene, its absorption spectrum shows a relatively larger increase in absorbance in going from the near-IR to visible region (Fig. 2). Absorption increases linearly with photon energy, though a small absorption band appears at 1.2 eV (≈1 μm) with an absorbance of nearly 4%. This band is attributed to the interband electronic transition from the valence band maximum (VBM) to the conduction band minimum (CBM) along the M–K–Γ direction. Note that the buckled antimonene shows negligible absorption in the visible region,[36] whereas relatively small visible light absorption is predicted for multilayer buckled antimonene.[37] For (atomically flat) multilayer antimonene, Table S2 (supplementary material) shows the stacking configurations to be degenerate with $\Delta E \leq 13$ meV, although the AA-stacked bilayer and the AAA-stacked trilayer can be considered as the energetically preferred configurations. Previously, the buckled multilayer antimonene was predicted to prefer ABC-stacking, though decreasing its interlayer separation, leads to either AAA- or ABA-stacking configurations with the energy difference of 113 meV/atom.[38]

We find that the calculated transmittance decreases as the thickness increases in going from monolayer to trilayer (Fig. S9, supplementary material). The decrease in transmission in the trilayer relative

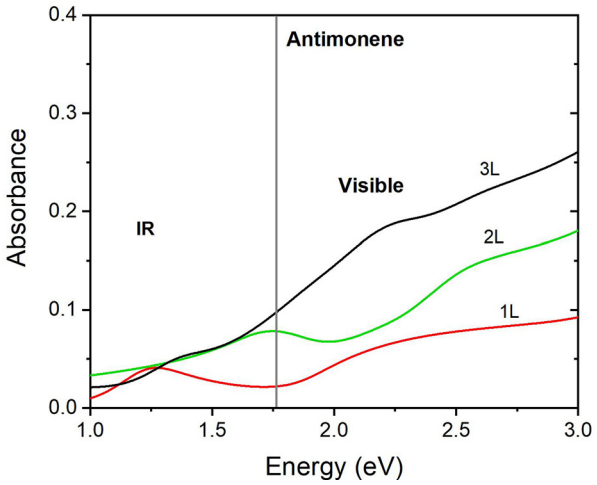

FIG. 2. Antimonene: absorbance as a function of the number of layers.

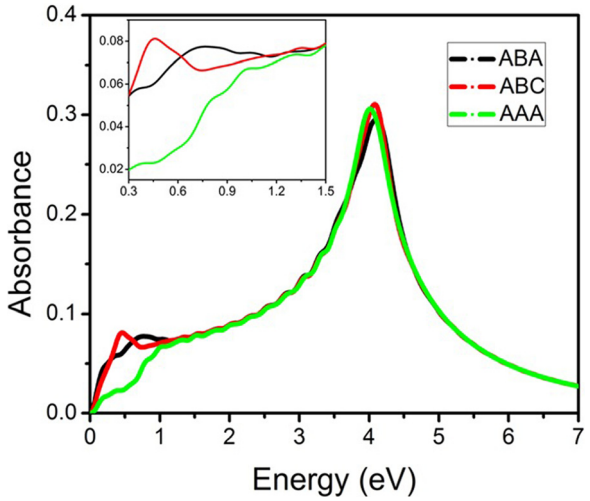

FIG. 3. Absorbance with the inset focusing on the mid-IR spectral region of trilayer graphene.

to the monolayer is about ≈25% for 400 nm and about ≈10% for 800 nm. The calculated refractive index of the planar antimonene varies with the thickness (Fig. S10, supplementary material) in contrast to the results obtained for multilayer graphene. At 400 nm, the calculated refractive index is 2.12 for monolayer and 2.2 for bilayer/trilayer antimonene. Note that the refractive index of the buckled β-antimonene is reported to be 2.0 for the UV spectral region.[39]

In multilayer graphene, a weak interlayer interaction allows a variety of stacking patterns to be formed; bilayer graphene can be arranged in either AB (Bernal) or AA (hexagonal) stacking configurations, whereas trilayer graphene may exist in ABA (Bernal), ABC (rhombohedral), or AAA (hexagonal) stacking configurations.[40] ABA-stacked trilayer graphene is predicted to be energetically stable as compared to ABC and AAA stacked trilayers. The energy difference (ΔE) is ≈4 meV and ≈51 meV for ABC- and AAA-stacked trilayers, respectively. Despite a rather small ΔE among the three stacking configurations, noticeable differences are seen in their IR absorbance, which suggests that the optical response can be influenced by topology (Fig. 3). For example, the ABC-stacked trilayer shows a prominent absorption band at 0.45 eV (≈2.75 μm) with absorbance significantly higher than that of the AAA-stacked trilayer (Fig. 3, inset). It should be noted that thermal effects, which were not included in the present study, can be a factor in modifying absorbance below 0.1 eV (≈12 μm).

To obtain further insight into the stacking-dependent absorption, we also calculated the low-energy electronic band structure around the K-point (Fig. S11, supplementary material). Here, the AAA-stacked trilayer shows a distinctly different electronic structure than the ABA or ABC stacked trilayer. The band structure of AAA-stacked graphene can be seen as a superposition of bands associated with individual layers, showing three Dirac cones near the Fermi level [Fig. S11(c)]. Due to a highly symmetric stacking pattern, the middle layer of graphene interacts equally with the top and the bottom layer, which results in a delocalized charge distribution associated with the middle layer. These results are in agreement with those reported in previous theoretical studies.[20,22,23,41,42] There exist two pairs of energy bands associated with VBM and CBM near the Fermi level for ABA stacking, and only one pair for ABC stacking. The other pairs of bands associated with VBM and CBM move away from the Fermi level which may lead to the prominent absorption at 0.45 eV as seen in Fig. S11(b), supplementary material. These stacking-dependent features may likely be associated with the number of uncoordinated atomic sites in adjacent layers; ABA stacking has two equidistant layers (top and bottom layers). This is reflected in the calculated charge density difference, $\Delta\rho = \rho_T - (\rho_{AB/AA} + \rho_{A/C})$ where ρ_T is the total charge density of the trilayer system, $\rho_{AB/AA}$ is the charge density of the AB or AA bilayer, and $\rho_{A/C}$ is the charge density of the top A or C layer of trilayer graphene (Fig. S12, supplementary material). A weak interlayer coupling between layers is seen in the charge density difference profile.

The topological dependence of the optical absorption calculated for trilayer antimonene is shown in Fig. S13. The absorption band in the visible region is at about 2.2 eV (≈0.56 μm) in AAA, 2.3 eV (≈0.54 μm) in ABA, and 2.0 eV (≈0.62 μm) in ABC stacked configurations, while a noticeable IR absorption at ∼0.5 eV (≈2.5 μm) appears only for ABA-stacked antimonene. To understand these features, we examine the low-energy electronic band structure along the Γ–K–M direction together with the partial density of states (Figs. S13–S15, supplementary material). The ≈2.5 μm bands are likely associated with the interband transition along the K–M direction for ABA-stacked antimonene. Analysis of the partial density of states suggests this transition be associated with the electric dipole allowed s → p transition in ABA-stacked antimonene. Note that a significant increase in the number of bands available for transition in trilayer antimonene leads to higher absorption compared to that calculated for the bilayer antimonene (Fig. S16, supplementary material).

The low-energy absorbance calculated for graphene and antimonene is compared in Fig. 4. Although, graphene and antimonene both are semi-metallic, a significant difference in their optical absorption is expected since the electronic configurations of C: [He] $2s^2 2p^2$ and Sb: [Kr] $4d^{10} 5s^2 5p^3$ differ significantly. In graphene, each C atom forms a covalent (σ) bond with each of its neighbors together with a π-bond oriented out-of-plane. On the other hand, in the case of antimonene,

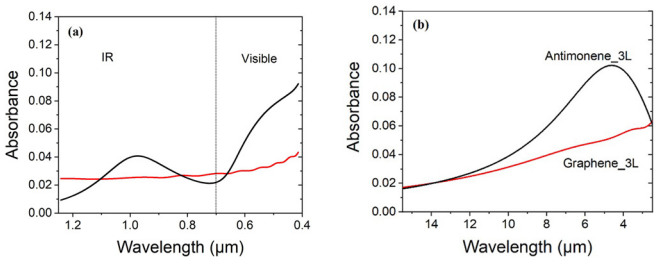

FIG. 4. (a) Absorbance of graphene and (atomically flat) antimonene and (b) IR absorbance of trilayer graphene and (atomically flat) antimonene. Color code: graphene in red and antimonene in black.

the out-of-plane component is the lone-pair electron on Sb atoms (Fig. S1, supplementary material), which may interact weakly with neighboring atoms as compared to the π-orbital interaction in the case of graphene, leading to the calculated difference in the absorption spectra of graphene and antimonene.

The difference in the electronic configurations of C and Sb is reflected in absorption in the visible spectral region where antimonene absorbs significantly higher than graphene; at 400 nm, absorbance is 3% and 9% for graphene and antimonene, respectively. The difference is further enhanced in the IR spectral region where a prominent, broadband appears at $\approx 4\,\mu$m for trilayer antimonene. This is not the case with trilayer graphene, for which a nearly linear decrease in absorption is predicted ranging from $2\,\mu$m to $15\,\mu$m. This suggests that multilayer antimonene could be a good candidate as a mid-IR tunable laser absorber.

In summary, absorbance in (atomically flat) multilayer antimonene is calculated to be comparable or greater than that for multilayer graphene. Specifically, the IR absorption in antimonene is significantly higher than that in graphene, with a prominent band at about $4\,\mu$m associated with the dipole-allowed interband transitions in the trilayer (atomically flat) antimonene. Overall, our study suggests multilayer graphene and antimonene are good optical absorbers, especially in the IR region of the spectrum, and can potentially be used as a coating for protection against mid-IR tunable lasers. Furthermore, the fabrication of antimonene/semiconductor heterostructures may open up the possibility of nanoscale applications for energy storage applications.

See the supplementary material for the molecular orbitals in graphene and antimonene; computational details—the convergence of k-point grid and vacuum distance; and results (figures and tables)—multilayer graphene: absorbance and transmittance, band structure, and refractive index; multilayer antimonene: absorbance and transmittance, refractive index, band structure, density of states, and charge density.

The authors thank Dr. Rahul Gupta, Dr. Aurora Costales, Dr. Matko Muzevic, Lisa Eggart, Dr. Pooja Jamdagni, Dr. Gaoxue Wang, and Dr. S. Gowtham for the helpful discussions. A.K. acknowledges the financial support provided by Michigan Technological University. Computational resources at Michigan Technological University with the SUPERIOR high-performance computing cluster were utilized. The research was partially supported by the Army Research Office (ARO) through Grant No. W911NF-14-2-0088.

DATA AVAILABILITY

The data that supports the findings of this study are available within the article (and its supplementary material).

REFERENCES

[1]J. Ji, X. Song, J. Liu, Z. Yan, C. Huo, S. Zhang, M. Su, L. Liao, W. Wang, and Z. Ni, "Two-dimensional antimonene single crystals grown by van der Waals epitaxy," Nat. Commun. **7**, 13352 (2016).
[2]J. Wang, Y. Hernandez, M. Lotya, J. N. Coleman, and W. J. Blau, "Broadband nonlinear optical response of graphene dispersions," Adv. Mater. **21**, 2430–2435 (2009).
[3]M. Feng, H. Zhan, and Y. Chen, "Nonlinear optical and optical limiting properties of graphene families," Appl. Phys. Lett. **96**, 033107 (2010).
[4]D. Dini, M. J. Calvete, and M. Hanack, "Nonlinear optical materials for the smart filtering of optical radiation," Chem. Rev. **116**, 13043–13233 (2016).
[5]G. Wang, S. Higgins, K. Wang, D. Bennett, N. Milosavljevic, J. J. Magan, S. Zhang, X. Zhang, J. Wang, and W. J. Blau, "Intensity-dependent nonlinear refraction of antimonene dispersions in the visible and near-infrared region," Appl. Opt. **57**, E147–E153 (2018).
[6]J. Guo, D. Huang, Y. Zhang, H. Yao, Y. Wang, F. Zhang, R. Wang, Y. Ge, Y. Song, and Z. Guo, "2D GeP as a novel broadband nonlinear optical material for ultrafast photonics," Laser Photonics Rev. **13**, 1900123 (2019).
[7]L. Matthes, P. Gori, O. Pulci, and F. Bechstedt, "Universal infrared absorbance of two-dimensional honeycomb group-IV crystals," Phys. Rev. B **87**, 035438 (2013).
[8]M. Gajdoš, K. Hummer, G. Kresse, J. Furthmüller, and F. Bechstedt, "Linear optical properties in the projector-augmented wave methodology," Phys. Rev. B **73**, 045112 (2006).
[9]E. Hendry, P. J. Hale, J. Moger, A. Savchenko, and S. A. Mikhailov, "Coherent nonlinear optical response of graphene," Phys. Rev. Lett. **105**, 097401 (2010).
[10]L. Kou, Y. Ma, X. Tan, T. Frauenheim, A. Du, and S. Smith, "Structural and electronic properties of layered arsenic and antimony arsenide," J. Phys. Chem. C **119**, 6918–6922 (2015).
[11]G. Wang, R. Pandey, and S. P. Karna, "Atomically thin group V elemental films: Theoretical investigations of antimonene allotropes," ACS Appl. Mater. Interfaces **7**, 11490–11496 (2015).
[12]T. Lei, C. Liu, J.-L. Zhao, J.-M. Li, Y.-P. Li, J.-O. Wang, R. Wu, H.-J. Qian, H.-Q. Wang, and K. Ibrahim, "Electronic structure of antimonene grown on Sb_2Te_3 (111) and Bi_2Te_3 substrates," J. Appl. Phys. **119**, 015302 (2016).
[13]X. Wu, Y. Shao, H. Liu, Z. Feng, Y. L. Wang, J. T. Sun, C. Liu, J. O. Wang, Z. L. Liu, and S. Y. Zhu, "Epitaxial growth and air-stability of monolayer antimonene on $PdTe_2$," Adv. Mater. **29**, 1605407 (2017).
[14]P. Ares, F. Aguilar-Galindo, D. Rodríguez-San-Miguel, D. A. Aldave, S. Díaz-Tendero, M. Alcamí, F. Martín, J. Gómez-Herrero, and F. Zamora, "Mechanical isolation of highly stable antimonene under ambient conditions," Adv. Mater. **28**, 6332–6336 (2016).
[15]Y. Shao, Z.-L. Liu, C. Cheng, X. Wu, H. Liu, C. Liu, J.-O. Wang, S.-Y. Zhu, Y.-Q. Wang, and D.-X. Shi, "Epitaxial growth of flat antimonene monolayer: A new honeycomb analogue of graphene," Nano Lett. **18**, 2133–2139 (2018).
[16]J. P. Perdew, K. Burke, and M. Ernzerhof, "Generalized gradient approximation made simple," Phys. Rev. Lett. **77**, 3865 (1996).
[17]S. Grimme, "Semiempirical GGA-type density functional constructed with a long-range dispersion correction," J. Comput. Chem. **27**, 1787–1799 (2006).
[18]R. R. Nair, P. Blake, A. N. Grigorenko, K. S. Novoselov, T. J. Booth, T. Stauber, N. M. Peres, and A. K. Geim, "Fine structure constant defines visual transparency of graphene," Science **320**, 1308–1308 (2008).
[19]Q. Bao, H. Zhang, Y. Wang, Z. Ni, Y. Yan, Z. X. Shen, K. P. Loh, and D. Y. Tang, "Atomic-layer graphene as a saturable absorber for ultrafast pulsed lasers," Adv. Funct. Mater. **19**, 3077–3083 (2009).
[20]K. F. Mak, M. Y. Sfeir, J. A. Misewich, and T. F. Heinz, "The evolution of electronic structure in few-layer graphene revealed by optical spectroscopy," Proc. Natl. Acad. Sci. **107**, 14999–15004 (2010).
[21]F. Ke, Y. Chen, K. Yin, J. Yan, H. Zhang, Z. Liu, S. T. John, J. Wu, H.-K. Mao, and B. Chen, "Large bandgap of pressurized trilayer graphene," Proc. Natl. Acad. Sci. **116**, 9186–9190 (2019).

[22]K. F. Mak, M. Y. Sfeir, Y. Wu, C. H. Lui, J. A. Misewich, and T. F. Heinz, "Measurement of the optical conductivity of graphene," Phys. Rev. Lett. **101**, 196405 (2008).
[23]K. F. Mak, J. Shan, and T. F. Heinz, "Electronic structure of few-layer graphene: Experimental demonstration of strong dependence on stacking sequence," Phys. Rev. Lett. **104**, 176404 (2010).
[24]C. H. Lui, Z. Li, K. F. Mak, E. Cappelluti, and T. F. Heinz, "Observation of an electrically tunable band gap in trilayer graphene," Nat. Phys. **7**, 944 (2011).
[25]B. Mohan, A. Kumar, and P. Ahluwalia, "A first principle study of interband transitions and electron energy loss in mono and bilayer graphene: Effect of the external electric field," Physica E **44**, 1670–1674 (2012).
[26]L. Yang, "First-principles study of the optical absorption spectra of electrically gated bilayer graphene," Phys. Rev. B **81**, 155445 (2010).
[27]M. U. Farooq, A. Hashmi, and J. Hong, "Thickness dependent optical properties of multilayer BN/graphene/BN," Surf. Sci. **634**, 25–30 (2015).
[28]A. Vela, M. Moutinho, F. Culchac, P. Venezuela, and R. B. Capaz, "Electronic structure and optical properties of twisted multilayer graphene," Phys. Rev. B **98**, 155135 (2018).
[29]L. Yang, J. Deslippe, C.-H. Park, M. L. Cohen, and S. G. Louie, "Excitonic effects on the optical response of graphene and bilayer graphene," Phys. Rev. Lett. **103**, 186802 (2009).
[30]M. He, C. Quan, C. He, Y. Huang, L. Zhu, Z. Yao, S. Zhang, J. Bai, and X. Xu, "Enhanced nonlinear saturable absorption of MoS_2/graphene nanocomposite films," J. Phys. Chem. C **121**, 27147–27153 (2017).
[31]P. Yadav, P. K. Srivastava, N. Ray, and S. Ghosh, "Robustness of the universal optical transmittance in monolayer and multilayer graphene flakes under Coulomb interactions," Phys. Rev. B **94**, 121406 (2016).
[32]M. Koshino, "Stacking-dependent optical absorption in multilayer graphene," New J. Phys. **15**, 015010 (2013).
[33]S.-E. Zhu, S. Yuan, and G. Janssen, "Optical transmittance of multilayer graphene," Europhys. Lett. **108**, 17007 (2014).
[34]V. Lucarini, J. J. Saarinen, K.-E. Peiponen, and E. M. Vartiainen, *Kramers-Kronig Relations in Optical Materials Research* (Springer Science & Business Media, 2005).
[35]J. You, S. Bongu, Q. Bao, and N. Panoiu, "Nonlinear optical properties and applications of 2D materials: Theoretical and experimental aspects," Nanophotonics **8**, 63–97 (2018).
[36]Y. Xu, B. Peng, H. Zhang, H. Shao, R. Zhang, and H. Zhu, "First-principle calculations of optical properties of monolayer arsenene and antimonene allotropes," Ann. Phys. **529**, 1600152 (2017).
[37]M. Mužević, M. V. Pajtler, S. K. Gupta, and I. Lukačević, "Modulation of optical properties with multilayer thickness in antimonene and indiene," Adv. Mater. Lett. **10**, 270–274 (2019).
[38]O. Ü. Aktürk, V. O. Özçelik, and S. Ciraci, "Single-layer crystalline phases of antimony: Antimonenes," Phys. Rev. B **91**, 235446 (2015).
[39]D. Singh, S. K. Gupta, Y. Sonvane, and I. Lukačević, "Antimonene: A monolayer material for ultraviolet optical nanodevices," J. Mater. Chem. C **4**, 6386–6390 (2016).
[40]C. Bao, W. Yao, E. Wang, C. Chen, J. Avila, M. C. Asensio, and S. Zhou, "Stacking-dependent electronic structure of trilayer graphene resolved by nano spot angle-resolved photoemission spectroscopy," Nano Lett. **17**, 1564–1568 (2017).
[41]H. Min and A. H. MacDonald, "Chiral decomposition in the electronic structure of graphene multilayers," Phys. Rev. B **77**, 155416 (2008).
[42]I. Lobato and B. Partoens, "Multiple Dirac particles in AA-stacked graphite and multilayers of graphene," Phys. Rev. B **83**, 165429 (2011).